Data-Driven Model Reduction for a Class of Semi-Explicit DAEs Using the Loewner Framework



Athanasios C. Antoulas, Ion Victor Gosea, and Matthias Heinkenschloss

Abstract This paper introduces a modified version of the recently proposed data-driven Loewner framework to compute reduced order models (ROMs) for a class of semi-explicit differential algebraic equation (DAE) systems, which include the semi-discretized linearized Navier–Stokes/Oseen equations. The modified version estimates the polynomial part of the original transfer function from data and incorporates this estimate into the Loewner ROM construction. Without this proposed modification the transfer function of the Loewner ROM is strictly proper, i.e., goes to zero as the magnitude of the frequency goes to infinity, and therefore may have a different behavior for large frequencies than the transfer function of the original system. The modification leads to a Loewner ROM with a transfer function that has a strictly proper and a polynomial part, just as the original model. This leads to better approximations for transfer function components in which the coefficients in the polynomial part are not too small. The construction of the improved Loewner ROM is described and the improvement is demonstrated on a large-scale system governed by the semi-discretized Oseen equations.

Keywords Model reduction · Loewner framework · Rational interpolation · Transfer function · Semi-explicit DAE · Oseen equations

A. C. Antoulas

Department of Electrical an Computer Engineering, Rice University, Houston, TX, USA

Max Planck Institute for Dynamics of Complex Technical Systems, Magdeburg, Germany e-mail: aca@rice.edu

I. V. Gosea (⊠)

Max Planck Institute for Dynamics of Complex Technical Systems, Magdeburg, Germany e-mail: gosea@mpi-magdeburg.mpg.de

M. Heinkenschloss

Department of Computational and Applied Mathematics, Rice University, Houston, TX, USA e-mail: heinken@rice.edu

 $\ensuremath{\mathbb{C}}$ The Editor(s) (if applicable) and The Author(s), under exclusive licence

to Springer Nature Switzerland AG 2020

T. Reis et al. (eds.), *Progress in Differential-Algebraic Equations II*, Differential-Algebraic Equations Forum,

https://doi.org/10.1007/978-3-030-53905-4_7

Mathematics Subject Classification (2010) 37M99, 37N10, 41A20, 93A15, 93B15, 93C15

1 Introduction

This paper introduces a modified version of the data-driven Loewner framework to compute reduced order models (ROMs) for a class of semi-explicit differential algebraic equation (DAE) systems, which includes systems arising from semi-discretized linearized Navier–Stokes/Oseen equations . The improvement is in the estimation of the polynomial part of the transfer function from measurements and in the incorporation of this estimate into the Loewner ROM construction, which in many cases leads to ROMs with better approximation properties.

Most ROM approaches first compute subspaces that contain the important dynamics of the system and then generate a ROM by applying a Galerkin or Petrov–Galerkin projection of the original full order model (FOM) onto these subspaces. These projection based ROM approaches include balanced truncation, interpolation based methods, proper orthogonal decomposition, reduced basis methods, and others. See, e.g., the books [1, 3, 5, 9, 12]. All of these ROM approaches require explicit access to the system matrices to apply the projection and generate the ROM. In contrast, the Loewner framework computes a ROM directly from measurements of the transfer function and does not require explicit knowledge of the system matrices. Thus, the Loewner framework can be applied even if the mathematical model of the system is not available, e.g., because proprietary software is used or measurements are generated directly from the physical system. The Loewner framework is described, e.g., in the book [3, Chapter 4] and in the recent survey [2].

The Loewner framework computes a ROM directly from transfer function measurements in such a way that the ROM transfer function approximately interpolates the transfer function of the original FOM at the measurements. However, the Loewner ROM generated with the original approach has a strictly proper transfer function. In particular, the ROM transfer function goes to zero as the magnitude of the frequency goes to infinity. In contrast, the transfer function of the original model may have a polynomial part which is bounded away from zero, or is even unbounded as the magnitude of the frequency goes to infinity. In this case, this substantially different behavior of transfer functions generates substantial differences away from the measurements, which means that the ROM may not capture important features of the original problem. As mentioned before, this paper shows how to estimate the polynomial part from transfer function measurements and how to incorporate these estimates into the Loewner ROM construction to generate better ROMs. In principle, there is no difference between the computation of a Loewner ROM for an ordinary differential equation (ODE) system and for a DAE system. However, for ODE systems the structure of the ODE system allows one to directly identify the polynomial part, especially assessing whether it is non-zero. Unfortunately, this is more involved for DAE systems. For theoretical purposes we derive the analytical

forms of the strictly proper and polynomial parts of the transfer function for our class of semi-explicit DAE systems. If available, the analytical form of the polynomial part of the transfer function could be used. However this requires access to the system matrices. As an alternative, we propose to estimate the polynomial part of the transfer function from measurements. We then show how to incorporate this estimate into the Loewner ROM construction to generate better ROMs. This paper specifically focuses on the structure of semi-explicit DAE systems arising, e.g., from semi-discretized Oseen equations and complements [7].

The class of semi-explicit DAE systems is given by

$$\mathbf{E}_{11}\frac{d}{dt}\mathbf{v}(t) = \mathbf{A}_{11}\mathbf{v}(t) + \mathbf{A}_{12}\mathbf{p}(t) + \mathbf{B}_{1,0}\mathbf{g}(t) + \mathbf{B}_{1,1}\frac{d}{dt}\mathbf{g}(t), \quad t \in (0, T),$$
(1.1a)

$$\mathbf{0} = \mathbf{A}_{12}^{T} \mathbf{v}(t) + \mathbf{B}_{2,0} \mathbf{g}(t), \qquad t \in (0, T),$$
(1.1b)

$$\mathbf{v}(0) = \mathbf{0},\tag{1.1c}$$

$$\mathbf{y}(t) = \mathbf{C}_1 \mathbf{v}(t) + \mathbf{C}_2 \mathbf{p}(t) + \mathbf{D}_0 \mathbf{g}(t) + \mathbf{D}_1 \frac{d}{dt} \mathbf{g}(t) \qquad t \in (0, T).$$
(1.1d)

Here \mathbf{v} , \mathbf{p} are the states (velocities and pressures in the Oseen system), \mathbf{g} are the inputs, and \mathbf{y} are the outputs. The matrix $\mathbf{E}_{11} \in \mathbb{R}^{n_v \times n_v}$ is symmetric positive definite, $\mathbf{A}_{11} \in \mathbb{R}^{n_v \times n_v}$, $\mathbf{A}_{12}^T \in \mathbb{R}^{n_p \times n_v}$, $n_p < n_v$, is a matrix with rank n_p , $\mathbf{B}_{1,0}$, $\mathbf{B}_{1,1} \in \mathbb{R}^{n_v \times n_g}$, $\mathbf{B}_{2,0} \in \mathbb{R}^{n_p \times n_g}$, $\mathbf{C}_1 \in \mathbb{R}^{n_y \times n_v}$, $\mathbf{C}_2 \in \mathbb{R}^{n_y \times n_p}$, and \mathbf{D}_0 , $\mathbf{D}_1 \in \mathbb{R}^{n_y \times n_g}$. See, e.g., the books [6, 10]. Derivatives $\frac{d}{dt}\mathbf{g}$ of the inputs appear in the semi-discretized equations, e.g., when inputs on the partial differential equation (PDE) level are given as Dirichlet conditions on the velocities (e.g., the input corresponds to suction/blowing actuation on the boundary).

Often it will be convenient to define $n = n_v + n_p$,

$$\mathbf{x}(t) = \begin{pmatrix} \mathbf{v}(t) \\ \mathbf{p}(t) \end{pmatrix}, \qquad \mathbf{E} = \begin{pmatrix} \mathbf{E}_{11} & \mathbf{0} \\ \mathbf{0} & \mathbf{0} \end{pmatrix}, \qquad \mathbf{A} = \begin{pmatrix} \mathbf{A}_{11} & \mathbf{A}_{12} \\ \mathbf{A}_{12}^T & \mathbf{0} \end{pmatrix}, \tag{1.2a}$$

$$\mathbf{B}_{0} = \begin{pmatrix} \mathbf{B}_{1,0} \\ \mathbf{B}_{2,0} \end{pmatrix}, \qquad \mathbf{B}_{1} = \begin{pmatrix} \mathbf{B}_{1,1} \\ \mathbf{0} \end{pmatrix}, \qquad \mathbf{C} = \begin{pmatrix} \mathbf{C}_{1} \ \mathbf{C}_{2} \end{pmatrix}, \tag{1.2b}$$

and write (1.1) in the compact notation

$$\mathbf{E}\frac{d}{dt}\mathbf{x}(t) = \mathbf{A}\mathbf{x}(t) + \mathbf{B}_0\mathbf{g}(t) + \mathbf{B}_1\frac{d}{dt}\mathbf{g}(t), \qquad t \in (0, T),$$
(1.3a)

$$\mathbf{E}\mathbf{x}(0) = \mathbf{0},\tag{1.3b}$$

$$\mathbf{y}(t) = \mathbf{C}\mathbf{x}(t) + \mathbf{D}_0\mathbf{g}(t) + \mathbf{D}_1\frac{d}{dt}\mathbf{g}(t), \qquad t \in (0, T).$$
 (1.3c)

This paper is organized as follows. In the next Sect. 2 we derive the analytical representations of the strictly proper and polynomial parts of the transfer function. Section 3 reviews the Loewner approach. Our approach for estimating the polynomial part of the transfer function from data is introduced in Sect. 4. Section 5 applies the Loewner approach with identification of the polynomial part of the transfer function to the Oseen equation.

2 Transfer Function

As mentioned before, the Loewner framework constructs a ROM such that its transfer function approximates the transfer function of the FOM. The transfer function $\mathbf{H}(s)$ of the FOM additively splits into a so-called strictly proper part $\mathbf{H}_{\mathrm{spr}}(s)$, which is a rational function in s with $\|\mathbf{H}_{\mathrm{spr}}(s)\| \to 0$ as $|s| \to \infty$, and a polynomial part $\mathbf{H}_{\mathrm{poly}}(s)$. Depending on the transfer function measurements available it can be difficult to obtain a good approximation of the combined transfer function

$$\mathbf{H}(s) = \mathbf{C}(s\,\mathbf{E} - \mathbf{A})^{-1}(\mathbf{B}_0 + s\,\mathbf{B}_1) + \mathbf{D}_0 + s\,\mathbf{D}_1 \tag{2.1}$$

associated with (1.3), and in these cases a separate approximation of the strictly proper and of the polynomial part can yield much better results. This section computes $\mathbf{H}_{\mathrm{spr}}(s)$ and $\mathbf{H}_{\mathrm{poly}}(s)$.

2.1 Transfer Function of an ODE System

First consider (1.3) with an invertible matrix E, i.e., consider an ODE system. Since

$$(s \mathbf{E} - \mathbf{A})^{-1} (\mathbf{B}_0 + s \mathbf{B}_1) = (s \mathbf{E} - \mathbf{A})^{-1} (\mathbf{B}_0 + \mathbf{A} \mathbf{E}^{-1} \mathbf{B}_1 + (s \mathbf{E} - \mathbf{A}) \mathbf{E}^{-1} \mathbf{B}_1)$$
$$= (s \mathbf{E} - \mathbf{A})^{-1} (\mathbf{B}_0 + \mathbf{A} \mathbf{E}^{-1} \mathbf{B}_1) + \mathbf{E}^{-1} \mathbf{B}_1,$$

the transfer function (2.1) can be written as

$$\mathbf{H}(s) = \underbrace{\mathbf{C}(s \mathbf{E} - \mathbf{A})^{-1}(\mathbf{B}_0 + \mathbf{A}\mathbf{E}^{-1}\mathbf{B}_1)}_{=\mathbf{H}_{\text{spr}}(s)} + \underbrace{\mathbf{C}\mathbf{E}^{-1}\mathbf{B}_1 + \mathbf{D}_0 + s \mathbf{D}_1}_{\mathbf{H}_{\text{poly}}(s)}.$$

If **E** is invertible, the strictly proper part and the polynomial part of the transfer function can be determined directly from the matrices in (1.3). Specifically, the polynomial part is at most linear,

$$\mathbf{H}_{\text{poly}}(s) = \mathbf{P}_0 + s \, \mathbf{P}_1$$
 with $\mathbf{P}_0 = \mathbf{C} \mathbf{E}^{-1} \mathbf{B}_1 + \mathbf{D}_0$, $\mathbf{P}_1 = \mathbf{D}_1$,

and the polynomial part is zero if B_1 , D_0 , D_1 are zero.

2.2 Transfer Function of the Semi-Explicit DAE System

Now consider (1.1). Because the corresponding **E** in (1.2) is singular, the representation (2.1) does not directly expose the strictly proper part and the polynomial part of the transfer function. We proceed as in [8] and transform (1.1) into an ODE system.

We write

$$\mathbf{v}(t) = \mathbf{v}_0(t) + \mathbf{v}_g(t), \tag{2.2}$$

where

$$\mathbf{v}_g(t) = -\mathbf{E}_{11}^{-1} \mathbf{A}_{12} (\mathbf{A}_{12}^T \mathbf{E}_{11}^{-1} \mathbf{A}_{12})^{-1} \mathbf{B}_{2,0} \mathbf{g}(t)$$
 (2.3)

is a particular solution of (1.1b) and $\mathbf{v}_0(t)$ satisfies $\mathbf{0} = \mathbf{A}_{12}^T \mathbf{v}_0(t)$. Furthermore, we define the projection

$$\mathbf{\Pi} = \mathbf{I} - \mathbf{A}_{12} (\mathbf{A}_{12}^T \mathbf{E}_{11}^{-1} \mathbf{A}_{12})^{-1} \mathbf{A}_{12}^T \mathbf{E}_{11}^{-1}.$$

It can be verified that $\Pi^2 = \Pi$, $\Pi \mathbf{E}_{11} = \mathbf{E}_{11}\Pi^T$, null(Π) = range(\mathbf{A}_{12}) and range(Π) = null($\mathbf{A}_{12}^T\mathbf{E}_{11}^{-1}$), i.e., Π is an \mathbf{E}_{11} -orthogonal projection. For (1.1) derived from a finite element discretization, Π is a discrete version of the Leray projector [4]. The properties of Π imply that

$$\mathbf{A}_{12}^T \mathbf{v}_0(t) = \mathbf{0} \quad \text{if and only if} \quad \mathbf{\Pi}^T \mathbf{v}_0(t) = \mathbf{v}_0(t). \tag{2.4}$$

Inserting (2.2), (2.3) into (1.1) gives

$$\mathbf{E}_{11} \frac{d}{dt} \mathbf{v}_{0}(t) = \mathbf{A}_{11} \mathbf{v}_{0}(t) + \mathbf{A}_{12} \mathbf{p}(t) + \mathbf{B}_{3} \mathbf{g}(t) + \left(\mathbf{B}_{1,1} + \mathbf{A}_{12} (\mathbf{A}_{12}^{T} \mathbf{E}_{11}^{-1} \mathbf{A}_{12})^{-1} \mathbf{B}_{2,0} \right) \frac{d}{dt} \mathbf{g}(t)$$
(2.5a)

$$\mathbf{0} = \mathbf{A}_{12}^T \mathbf{v}_0(t), \tag{2.5b}$$

$$\mathbf{v}_0(0) = -\mathbf{v}_g(0),\tag{2.5c}$$

$$\mathbf{y}(t) = \mathbf{C}_{1}\mathbf{v}_{0}(t) + \mathbf{C}_{2}\mathbf{p}(t) + \left(\mathbf{D}_{0} - \mathbf{C}_{1}\mathbf{E}_{11}^{-1}\mathbf{A}_{12}(\mathbf{A}_{12}^{T}\mathbf{E}_{11}^{-1}\mathbf{A}_{12})^{-1}\mathbf{B}_{2,0}\right)\mathbf{g}(t)$$

$$+ \mathbf{D}_{1}\frac{d}{dt}\mathbf{g}(t), \tag{2.5d}$$

where

$$\mathbf{B}_{3} := \mathbf{B}_{1,0} - \mathbf{A}_{11} \mathbf{E}_{11}^{-1} \mathbf{A}_{12} (\mathbf{A}_{12}^{T} \mathbf{E}_{11}^{-1} \mathbf{A}_{12})^{-1} \mathbf{B}_{2,0}. \tag{2.6}$$

Next we express \mathbf{p} in terms of \mathbf{v}_0 and project onto the constraint (2.5b). Specifically, we multiply (2.5a) by $\mathbf{A}_{12}^T \mathbf{E}_{11}^{-1}$, then use (2.5b) and finally solve the resulting equation for \mathbf{p} to get

$$\mathbf{p}(t) = -\left(\mathbf{A}_{12}^{T} \mathbf{E}_{11}^{-1} \mathbf{A}_{12}\right)^{-1} \mathbf{A}_{12}^{T} \mathbf{E}_{11}^{-1} \mathbf{A}_{11} \mathbf{v}_{0}(t)$$

$$-\left(\mathbf{A}_{12}^{T} \mathbf{E}_{11}^{-1} \mathbf{A}_{12}\right)^{-1} \mathbf{A}_{12}^{T} \mathbf{E}_{11}^{-1} \mathbf{B}_{3} \mathbf{g}(t)$$

$$-\left(\mathbf{A}_{12}^{T} \mathbf{E}_{11}^{-1} \mathbf{A}_{12}\right)^{-1} \left(\mathbf{A}_{12}^{T} \mathbf{E}_{11}^{-1} \mathbf{B}_{1,1} + \mathbf{B}_{2,0}\right) \frac{d}{dt} \mathbf{g}(t). \tag{2.7}$$

Now we insert (2.7) into (2.5d), apply (2.4), and use $\mathbf{\Pi} \mathbf{A}_{12} (\mathbf{A}_{12}^T \mathbf{E}_{11}^{-1} \mathbf{A}_{12})^{-1} = \mathbf{0}$ to write (2.5) as

$$\boldsymbol{\Pi}\mathbf{E}_{11}\boldsymbol{\Pi}^{T}\frac{d}{dt}\mathbf{v}_{0}(t) = \boldsymbol{\Pi}\mathbf{A}_{11}\boldsymbol{\Pi}^{T}\mathbf{v}_{0}(t) + \boldsymbol{\Pi}\mathbf{B}_{3}\mathbf{g}(t) + \boldsymbol{\Pi}\mathbf{B}_{1,1}\frac{d}{dt}\mathbf{g}(t), \quad t \in (0, T),$$
(2.8a)

$$\boldsymbol{\Pi}^T \mathbf{v}_0(0) = -\boldsymbol{\Pi}^T \mathbf{v}_g(0), \tag{2.8b}$$

$$\mathbf{y}(t) = \mathbf{C}_3 \boldsymbol{\Pi}^T \mathbf{v}_0(t) + \widetilde{\mathbf{P}}_0 \mathbf{g}(t) + \mathbf{P}_1 \frac{d}{dt} \mathbf{g}(t), \qquad t \in (0, T),$$
(2.8c)

where \mathbf{B}_3 is given by (2.6) and

$$\mathbf{C}_3 := \mathbf{C}_1 - \mathbf{C}_2 (\mathbf{A}_{12}^T \mathbf{E}_{11}^{-1} \mathbf{A}_{12})^{-1} \mathbf{A}_{12}^T \mathbf{E}_{11}^{-1} \mathbf{A}_{11}, \tag{2.9a}$$

$$\widetilde{\mathbf{P}}_0 := \mathbf{D}_0 - \mathbf{C}_1 \mathbf{E}_{11}^{-1} \mathbf{A}_{12} (\mathbf{A}_{12}^T \mathbf{E}_{11}^{-1} \mathbf{A}_{12})^{-1} \mathbf{B}_{2,0}$$

$$-\mathbf{C}_{2}(\mathbf{A}_{12}^{T}\mathbf{E}_{11}^{-1}\mathbf{A}_{12})^{-1}\mathbf{A}_{12}^{T}\mathbf{E}_{11}^{-1}\mathbf{B}_{3},\tag{2.9b}$$

$$\mathbf{P}_{1} := \mathbf{D}_{1} - \mathbf{C}_{2} (\mathbf{A}_{12}^{T} \mathbf{E}_{11}^{-1} \mathbf{A}_{12})^{-1} (\mathbf{A}_{12}^{T} \mathbf{E}_{11}^{-1} \mathbf{B}_{1,1} + \mathbf{B}_{2,0}). \tag{2.9c}$$

The system (2.8) is a dynamical system in the $n_v - n_p$ dimensional subspace null(Π) and (2.8a,b) has to be solved for $\Pi^T \mathbf{v} = \mathbf{v}$. This can be made more explicit by decomposing

$$\boldsymbol{\Pi} = \boldsymbol{\Theta}_l \boldsymbol{\Theta}_r^T \tag{2.10a}$$

with $\boldsymbol{\Theta}_l, \boldsymbol{\Theta}_r \in \mathbb{R}^{n_v \times (n_v - n_p)}$ satisfying

$$\mathbf{\Theta}_{I}^{T}\mathbf{\Theta}_{r} = \mathbf{I}.\tag{2.10b}$$

Substituting this decomposition into (2.8) shows that $\tilde{\mathbf{v}}_0 = \boldsymbol{\Theta}_l^T \mathbf{v}_0 \in \mathbb{R}^{n_v - n_p}$ must satisfy

$$\boldsymbol{\Theta}_{r}^{T} \mathbf{E}_{11} \boldsymbol{\Theta}_{r} \frac{d}{dt} \widetilde{\mathbf{v}}_{0}(t) = \boldsymbol{\Theta}_{r}^{T} \mathbf{A}_{11} \boldsymbol{\Theta}_{r} \widetilde{\mathbf{v}}_{0}(t)$$

$$+ \boldsymbol{\Theta}_{r}^{T} \mathbf{B}_{3} \mathbf{g}(t) + \boldsymbol{\Theta}_{r}^{T} \mathbf{B}_{1,1} \frac{d}{dt} \mathbf{g}(t), \qquad t \in (0, T), \qquad (2.11a)$$

$$\widetilde{\mathbf{v}}_{0}(0) = - \boldsymbol{\Theta}_{l}^{T} \mathbf{v}_{\varrho}(0), \qquad (2.11b)$$

$$\mathbf{y}(t) = \mathbf{C}_3 \boldsymbol{\Theta}_r \widetilde{\mathbf{v}}_0(t) + \widetilde{\mathbf{P}}_0 \mathbf{g}(t) + \mathbf{P}_1 \frac{d}{dt} \mathbf{g}(t), \quad t \in (0, T).$$
 (2.11c)

The systems (1.1) and (2.11) are equivalent. Again we refer to [8] for details. Specifically, the transfer function of (1.1) is identical to the transfer function of (2.11). Since the $(n_v - n_p) \times (n_v - n_p)$ matrix $\boldsymbol{\Theta}_r^T \mathbf{E}_{11} \boldsymbol{\Theta}_r$ has full rank, we can proceed as in Sect. 2.1 to read off the strictly proper part and the polynomial part of the transfer function from the system representation (2.11),

$$\mathbf{H}(s) = \mathbf{H}_{\text{spr}}(s) + \mathbf{H}_{\text{poly}}(s), \tag{2.12a}$$

where

$$\mathbf{H}_{\text{spr}}(s) = \mathbf{C}_{3} \boldsymbol{\Theta}_{r} \left(s \; \boldsymbol{\Theta}_{r}^{T} \mathbf{E}_{11} \boldsymbol{\Theta}_{r} - \boldsymbol{\Theta}_{r}^{T} \mathbf{A}_{11} \boldsymbol{\Theta}_{r} \right)^{-1} \times \left(\boldsymbol{\Theta}_{r}^{T} \mathbf{B}_{3} + \boldsymbol{\Theta}_{r}^{T} \mathbf{A}_{11} \boldsymbol{\Theta}_{r} (\boldsymbol{\Theta}_{r}^{T} \mathbf{E}_{11} \boldsymbol{\Theta}_{r})^{-1} \boldsymbol{\Theta}_{r}^{T} \mathbf{B}_{1,1} \right), \tag{2.12b}$$

$$\mathbf{H}_{\text{poly}}(s) = \underbrace{\mathbf{C}_{3}\boldsymbol{\Theta}_{r} \left(\boldsymbol{\Theta}_{r}^{T} \mathbf{E}_{11} \boldsymbol{\Theta}_{r}\right)^{-1} \boldsymbol{\Theta}_{r}^{T} \mathbf{B}_{1,1} + \widetilde{\mathbf{P}}_{0}}_{=\mathbf{P}_{0}} + s \, \mathbf{P}_{1}. \tag{2.12c}$$

Thus the polynomial part of the transfer function of (1.1) is again at most linear, but the matrices P_0 and P_1 are more involved.

If the system matrices \mathbf{E}_{11}, \ldots in (1.1) are available then the matrices in (2.6) and (2.9) and the matrices \mathbf{P}_0 and \mathbf{P}_1 in (2.12c) can be computed using results already applied in [8]. We summarize these results next. However, if one does not have

access to the system matrices E_{11} , ... one needs to estimate the polynomial parts P_0 and P_1 from transfer function measurements, as we will describe in Sect. 4.

2.3 Computational Details

If

$$\begin{pmatrix} \mathbf{E}_{11} \ \mathbf{A}_{12} \\ \mathbf{A}_{12}^T \ \mathbf{0} \end{pmatrix} \begin{pmatrix} \mathbf{X}_1 \\ \mathbf{Z}_1 \end{pmatrix} = \begin{pmatrix} \mathbf{0} \\ \mathbf{B}_{2,0} \end{pmatrix}, \quad \begin{pmatrix} \mathbf{E}_{11} \ \mathbf{A}_{12} \\ \mathbf{A}_{12}^T \ \mathbf{0} \end{pmatrix} \begin{pmatrix} \mathbf{X}_2 \\ \mathbf{Z}_2 \end{pmatrix} = \begin{pmatrix} \mathbf{0} \\ \mathbf{C}_2 \end{pmatrix}, \quad (2.13)$$

then $\mathbf{X}_1^T = \mathbf{B}_{2,0}^T (\mathbf{A}_{12}^T \mathbf{E}_{11}^{-1} \mathbf{A}_{12})^{-1} \mathbf{A}_{12}^T \mathbf{E}_{11}^{-1}$, $\mathbf{Z}_1^T = -\mathbf{B}_{2,0} (\mathbf{A}_{12}^T \mathbf{E}_{11}^{-1} \mathbf{A}_{12})^{-1}$, and $\mathbf{X}_2^T = \mathbf{C}_2^T (\mathbf{A}_{12}^T \mathbf{E}_{11}^{-1} \mathbf{A}_{12})^{-1} \mathbf{A}_{12}^T \mathbf{E}_{11}^{-1}$, $\mathbf{Z}_2^T = -\mathbf{C}_2 (\mathbf{A}_{12}^T \mathbf{E}_{11}^{-1} \mathbf{A}_{12})^{-1}$. Hence, the matrices in (2.6) and (2.9) can be written as

$$\mathbf{B}_3 = \mathbf{B}_{1,0} - \mathbf{A}_{11}\mathbf{X}_1, \qquad \mathbf{C}_3 = \mathbf{C}_1 - \mathbf{X}_2^T\mathbf{A}_{11},$$

and

$$\tilde{\mathbf{P}}_0 = \mathbf{D}_0 - \mathbf{C}_1 \mathbf{X}_1 - \mathbf{X}_2^T \mathbf{B}_3, \qquad \mathbf{P}_1 = \mathbf{D}_1 - \mathbf{X}_2^T \mathbf{B}_{1,1} + \mathbf{Z}_2^T \mathbf{B}_{2,0}.$$

If

$$\begin{pmatrix} \mathbf{E}_{11} \ \mathbf{A}_{12} \\ \mathbf{A}_{12}^T \ \mathbf{0} \end{pmatrix} \begin{pmatrix} \mathbf{X}_3 \\ \mathbf{Z}_3 \end{pmatrix} = \begin{pmatrix} \mathbf{B}_{1,1} \\ \mathbf{0} \end{pmatrix}, \tag{2.14}$$

then P_0 in (2.12c) can be written as

$$\mathbf{P}_0 = \widetilde{\mathbf{P}}_0 + \mathbf{C}_3 \mathbf{X}_3.$$

In fact, $\mathbf{A}_{12}^T \mathbf{X}_3 = \mathbf{0}$ implies $\mathbf{X}_3 = \boldsymbol{\Pi}^T \mathbf{X}_3 = \boldsymbol{\Theta}_r \boldsymbol{\Theta}_l^T \mathbf{X}_3$ by (2.4) and (2.10a). Hence, with $\widetilde{\mathbf{X}}_3 = \boldsymbol{\Theta}_l^T \mathbf{X}_3$ the first block in (2.14) reads $\mathbf{E}_{11} \boldsymbol{\Theta}_r \widetilde{\mathbf{X}}_3 + \mathbf{A}_{12} \mathbf{Z}_3 = \mathbf{B}_{1,1}$. Since $\text{null}(\boldsymbol{\Theta}_r^T) = \text{null}(\boldsymbol{\Pi}) = \text{range}(\mathbf{A}_{12}), \ \boldsymbol{\Theta}_r^T \mathbf{E}_{11} \boldsymbol{\Theta}_r \widetilde{\mathbf{X}}_3 = \boldsymbol{\Theta}_r^T \mathbf{B}_{1,1}$. This gives $\mathbf{C}_3 \boldsymbol{\Theta}_r (\boldsymbol{\Theta}_r^T \mathbf{E}_{11} \boldsymbol{\Theta}_r)^{-1} \boldsymbol{\Theta}_r^T \mathbf{B}_{1,1} = \mathbf{C}_3 \boldsymbol{\Theta}_r \widetilde{\mathbf{X}}_3 = \mathbf{C}_3 \mathbf{X}_3$.

3 Loewner Framework Applied to the Oseen Equations

We review the Loewner framework applied to (1.3). The presentation is standard and follows the recent tutorial paper [2] and book [3, Chapter 4]. In the next Sect. 4 we modify it to better account for the presence of a polynomial part in the transfer function (2.12).

The Loewner framework (LF) is a data-driven model identification and reduction technique that was originally introduced in [11] and was continuously developed, improved and extended to different problems and system classes during the last decade. It is an interpolation-based method that produces ROMs that (approximately) interpolate the transfer function corresponding to the underlying FOM at the given interpolation frequencies. Unlike other interpolation-based methods the LF computes the ROM from measurements of the transfer function rather than by projection of the original system.

Let $m = n_g$ be the number of inputs and $p = n_y$ be the number of outputs, so that $\mathbf{H}(s) \in \mathbb{C}^{p \times m}$. We assume that given frequencies

$$\mu_j, \ \lambda_j \in \mathbb{C}, \qquad j = 1, \dots, N,$$
 (3.1a)

left tangential directions

$$\ell_j \in \mathbb{C}^p, \qquad j = 1, \dots, N,$$
 (3.1b)

and right tangential directions

$$\mathbf{r}_j \in \mathbb{C}^m \qquad j = 1, \dots, N,$$
 (3.1c)

we have transfer function measurements

$$\mathbf{v}_{j}^{*} := \boldsymbol{\ell}_{j}^{*} \mathbf{H}(\mu_{j}) \in \mathbb{C}^{1 \times m}, \qquad \mathbf{w}_{j} := \mathbf{H}(\lambda_{j}) \mathbf{r}_{j} \in \mathbb{C}^{p \times 1}, \quad j = 1, \dots, N.$$
(3.1d)

We seek a ROM of the form¹

$$\widehat{\mathbf{E}}\frac{d}{dt}\widehat{\mathbf{x}}(t) = \widehat{\mathbf{A}}\widehat{\mathbf{x}}(t) + \widehat{\mathbf{B}}_0\mathbf{g}(t) + \widehat{\mathbf{B}}_1\frac{d}{dt}\mathbf{g}(t), \qquad t \in (0, T),$$
(3.2a)

$$\widehat{\mathbf{E}}\widehat{\mathbf{x}}(0) = \mathbf{0},\tag{3.2b}$$

$$\widehat{\mathbf{y}}(t) = \widehat{\mathbf{C}}\widehat{\mathbf{x}}(t) + \widehat{\mathbf{P}}_0 \mathbf{g}(t) + \widehat{\mathbf{P}}_1 \frac{d}{dt} \mathbf{g}(t), \qquad t \in (0, T),$$
(3.2c)

where $\widehat{\mathbf{E}}$ and $\widehat{\mathbf{A}}$ are of size $r \times r$ with small r, $\widehat{\mathbf{B}}_0$, $\widehat{\mathbf{B}}_0$ have r rows, and $\widehat{\mathbf{C}}$ has r columns, such that the corresponding transfer function $\widehat{\mathbf{H}}$ is an approximate tangential interpolant to the original transfer function \mathbf{H} , i.e., such that

$$\boldsymbol{\ell}_{j}^{*}\widehat{\boldsymbol{H}}(\mu_{j}) \approx \boldsymbol{\ell}_{j}^{*}\mathbf{H}(\mu_{j}) = \mathbf{v}_{j}^{*} \quad \text{for} \quad j = 1, \dots, N,
\widehat{\boldsymbol{H}}(\lambda_{j})\mathbf{r}_{j} \approx \mathbf{H}(\lambda_{j})\mathbf{r}_{j} = \mathbf{w}_{j} \quad \text{for} \quad j = 1, \dots, N.$$
(3.3)

¹The matrices $\widehat{\mathbf{E}}$ and $\widehat{\mathbf{A}}$ do not have the block 2×2 structure of \mathbf{E} and \mathbf{A} in (1.2).

Because of the left and right tangential interpolation conditions $\{\mu_j\}_{j=1}^N \subset \mathbb{C}$ are called the left interpolation points, $\{\mathbf{v}_j\}_{j=1}^N \subset \mathbb{C}^m$ are called the left sample values, $\{\boldsymbol{\ell}_j\}_{j=1}^N \subset \mathbb{C}^p$ are called the left tangential directions and $\{\lambda_j\}_{j=1}^N \subset \mathbb{C}$ are called the right interpolation points, $\{\mathbf{w}_j\}_{j=1}^N \subset \mathbb{C}^p$ are called the right sample values, $\{\mathbf{r}_j\}_{j=1}^N \subset \mathbb{C}^m$ are called the right tangential directions.

We assume that the left interpolation points and the right interpolation points are distinct, i.e. that

$$\{\mu_j\}_{j=1}^N \cap \{\lambda_j\}_{j=1}^N = \emptyset.$$

The measured data are arranged into matrix format as follows²

$$\mathbf{M} = \operatorname{diag}(\mu_{1}, \mu_{2}, \dots, \mu_{N}) \in \mathbb{C}^{N \times N}, \quad \mathbf{\Lambda} = \operatorname{diag}(\lambda_{1}, \lambda_{2}, \dots, \lambda_{N}) \in \mathbb{C}^{N \times N},$$

$$\mathbf{L}^{*} = \begin{bmatrix} \boldsymbol{\ell}_{1} \ \boldsymbol{\ell}_{2} \cdots \boldsymbol{\ell}_{N} \end{bmatrix} \in \mathbb{C}^{p \times N}, \quad \mathbf{R} = \begin{bmatrix} \mathbf{r}_{1} \ \mathbf{r}_{2} \cdots \mathbf{r}_{N} \end{bmatrix} \in \mathbb{C}^{m \times N}, \quad (3.4)$$

$$\mathbf{V}^{*} = \begin{bmatrix} \mathbf{v}_{1} \ \mathbf{v}_{2} \cdots \mathbf{v}_{N} \end{bmatrix} \in \mathbb{C}^{m \times N}, \quad \mathbf{W} = \begin{bmatrix} \mathbf{w}_{1} \ \mathbf{w}_{2} \cdots \mathbf{w}_{N} \end{bmatrix} \in \mathbb{C}^{p \times N}.$$

The Loewner matrix is given by

$$\mathbb{L} = \begin{bmatrix} \frac{\mathbf{v}_{1}^{*}\mathbf{r}_{1} - \boldsymbol{\ell}_{1}^{*}\mathbf{w}_{1}}{\mu_{1} - \lambda_{1}} & \cdots & \frac{\mathbf{v}_{1}^{*}\mathbf{r}_{N} - \boldsymbol{\ell}_{1}^{*}\mathbf{w}_{N}}{\mu_{1} - \lambda_{N}} \\ \vdots & \ddots & \vdots \\ \frac{\mathbf{v}_{N}^{*}\mathbf{r}_{1} - \boldsymbol{\ell}_{N}^{*}\mathbf{w}_{1}}{\mu_{N} - \lambda_{1}} & \cdots & \frac{\mathbf{v}_{N}^{*}\mathbf{r}_{N} - \boldsymbol{\ell}_{N}^{*}\mathbf{w}_{N}}{\mu_{N} - \lambda_{N}} \end{bmatrix} \in \mathbb{C}^{N \times N}.$$

$$(3.5)$$

Using (3.4) it can be verified that the Loewner matrix (3.5) solves the Sylvester equation

$$\mathbf{M} \mathbb{L} - \mathbb{L} \mathbf{\Lambda} = \mathbf{V} \mathbf{R} - \mathbf{L} \mathbf{W}.$$

The shifted Loewner matrix is given by

$$\mathbb{L}_{s} = \begin{bmatrix} \frac{\mathbf{v}_{1}^{T} \mathbf{r}_{1} \mu_{1} - \boldsymbol{\ell}_{1}^{*} \mathbf{w}_{1} \lambda_{1}}{\mu_{1} - \lambda_{1}} & \cdots & \frac{\mathbf{v}_{1}^{*} \mathbf{r}_{N} \mu_{1} - \boldsymbol{\ell}_{1}^{*} \mathbf{w}_{N} \lambda_{N}}{\mu_{1} - \lambda_{N}} \\ \vdots & \ddots & \vdots \\ \frac{\mathbf{v}_{N}^{*} \mathbf{r}_{1} \mu_{N} - \boldsymbol{\ell}_{N}^{*} \mathbf{w}_{1} \lambda_{1}}{\mu_{N} - \lambda_{1}} & \cdots & \frac{\mathbf{v}_{N}^{*} \mathbf{r}_{N} \mu_{N} - \boldsymbol{\ell}_{N}^{*} \mathbf{w}_{N} \lambda_{N}}{\mu_{N} - \lambda_{N}} \end{bmatrix} \in \mathbb{C}^{N \times N}.$$

$$(3.6)$$

²Note that the matrices $\mathbf{V}^* \in \mathbb{C}^{m \times N}$ and $\mathbf{W} \in \mathbb{C}^{p \times N}$ contain transfer function measurements (3.1) and are not projection matrices.

Using (3.4) it can be verified that the shifted Loewner matrix (3.6) solves the Sylvester equation

$$\mathbf{M}\mathbb{L}_{s} - \mathbb{L}_{s}\mathbf{\Lambda} = \mathbf{MVR} - \mathbf{LW}\mathbf{\Lambda}.$$

If the 'right' amount of data is given,³ then the ROM computed with the (classical) Loewner method is (3.2) with

$$\widehat{\mathbf{E}} = -\mathbb{L}, \ \widehat{\mathbf{A}} = -\mathbb{L}_s, \ \widehat{\mathbf{B}}_0 = \mathbf{V}, \ \widehat{\mathbf{B}}_1 = \mathbf{0}, \ \widehat{\mathbf{C}} = \mathbf{W}, \ \widehat{\mathbf{P}}_0 = \widehat{\mathbf{P}}_1 = \mathbf{0}.$$
 (3.7)

The ROM (3.2) with (3.7) is in general complex. However, if the data (3.1) contain also the conjugate complex data $(\{\mu_j\}_{j=1}^N = \{\overline{\mu}_j\}_{j=1}^N, \{\lambda_j\}_{j=1}^N = \{\overline{\lambda}_j\}_{j=1}^N$, etc.), then the complex ROM (3.7) can be transformed into a real ROM with the same transfer function, as shown in [2, p. 360]. The transfer function $\widehat{\boldsymbol{H}}$ corresponding to (3.7) satisfies the interpolation conditions (3.3) with equality. However, while it satisfies the interpolation conditions (3.3), the transfer function $\widehat{\boldsymbol{H}}$ by design is strictly proper, $\widehat{\boldsymbol{H}}_{\text{poly}} = \boldsymbol{0}$, and therefore the error $\boldsymbol{H} - \widehat{\boldsymbol{H}}$ is large, especially for large frequency. We will address this deficiency in Sect. 4.

Often more data than necessary are provided and the pencil (\mathbb{L}_s , \mathbb{L}) is singular. In this case we use the singular value decomposition (SVD) to extract the important information. Specifically, we compute the (short) SVDs of the augmented Loewner matrices as

$$\begin{bmatrix} \mathbb{L} & \mathbb{L}_s \end{bmatrix} = \mathbf{Y}_1 \mathbf{S}_1 \mathbf{X}_1^*, \quad \begin{bmatrix} \mathbb{L} \\ \mathbb{L}_s \end{bmatrix} = \mathbf{Y}_2 \mathbf{S}_2 \mathbf{X}_2^*, \tag{3.8}$$

where $\mathbf{S}_1 = \operatorname{diag}(\sigma_1^{(1)}, \dots, \sigma_N^{(1)}) \in \mathbb{R}^{N \times N}$ and $\mathbf{S}_2 = \operatorname{diag}(\sigma_1^{(2)}, \dots, \sigma_N^{(2)}) \in \mathbb{R}^{N \times N}$ are the matrices with singular values on the diagonal, and $\mathbf{Y}_1, \mathbf{X}_2 \in \mathbb{C}^{N \times N}, \mathbf{Y}_2, \mathbf{X}_1 \in \mathbb{C}^{2N \times N}$ are the matrices of singular vectors.

The size r of the ROM can be chosen as follows. Given a tolerance $\tau>0$ the truncation order r is the smallest integer such that the normalized singular values satisfy $\sigma_j^{(1)}/\sigma_1^{(1)} < \tau, \sigma_j^{(2)}/\sigma_1^{(2)} < \tau, j=r+1,\ldots,N$.

The matrices $\mathbf{Y}, \mathbf{X} \in \mathbb{C}^{N \times r}$ are obtained by selecting the first r columns of the matrices \mathbf{Y}_1 and \mathbf{X}_2 . The reduced Loewner system is constructed by multiplying the matrices \mathbb{L} , \mathbb{L}_s , \mathbf{V} , \mathbf{W} with \mathbf{Y}^* and \mathbf{X} to the left and respectively, to the right, as

$$\widehat{\mathbb{L}} = \mathbf{Y}^* \mathbb{L} \mathbf{X}, \quad \widehat{\mathbb{L}}_s = \mathbf{Y}^* \mathbb{L}_s \mathbf{X}, \quad \widehat{\mathbf{V}} = \mathbf{Y}^* \mathbf{V}, \quad \widehat{\mathbf{W}} = \mathbf{W} \mathbf{X}.$$
 (3.9)

³What the 'right' amount of data is depends on the transfer function. Since we typically have more data, the case we describe below, we omit specification of the 'right' amount of data.

The ROM computed with the (classical) Loewner method is (3.2) with

$$\widehat{\mathbf{E}} = -\widehat{\mathbb{L}}, \ \widehat{\mathbf{A}} = -\widehat{\mathbb{L}}_s, \ \widehat{\mathbf{B}}_0 = \widehat{\mathbf{V}}, \ \widehat{\mathbf{B}}_1 = \mathbf{0}, \ \widehat{\mathbf{C}} = \widehat{\mathbf{W}}, \ \widehat{\mathbf{P}}_0 = \widehat{\mathbf{P}}_1 = \mathbf{0}.$$
 (3.10)

As before, if the data $\{\mu_j\}_{j=1}^N$, $\{\lambda_i\}_{i=1}^N$, $\{\mathbf{v}_j\}_{j=1}^N$, $\{\mathbf{w}_j\}_{i=1}^N$ contain also the conjugate complex data, then the complex ROM (3.2) with (3.10) can be transformed into a real ROM with the same transfer function, as shown in [2, p. 360].

The transfer function \hat{H} corresponding to (3.10) satisfies the approximate interpolation conditions (3.3). However, by design, the transfer function \hat{H} is strictly proper, $\hat{H}_{\text{poly}} = \mathbf{0}$, and therefore the error $\mathbf{H} - \hat{H}$ is large, especially for large frequency. We will address this deficiency next.

4 Accounting for the Polynomial Part of the Transfer Function

As we have seen in Sect. 2.2, the transfer function is composed of a strictly proper part and a polynomial part. The exact structure of these parts is shown in (2.12). We write $\mathbf{H}(s) = \mathbf{H}_{\rm spr}(s) + \mathbf{H}_{\rm poly}(s)$ with

$$\mathbf{H}_{\text{poly}}(s) = \mathbf{P}_0 + s\mathbf{P}_1.$$

Especially for the DAE system (1.1), the exact form (2.12) of \mathbf{P}_0 , $\mathbf{P}_1 \in \mathbb{R}^{p \times m}$ is complicated. Here, as in Sect. 3, $m = n_g$ is the number of inputs and $p = n_y$ is the number of outputs, so that $\mathbf{H}(s) \in \mathbb{C}^{p \times m}$. Even if all system matrices in (1.1) were available, the computation of \mathbf{P}_0 , $\mathbf{P}_1 \in \mathbb{R}^{p \times m}$ from (2.12) is tedious. More importantly, if only transfer function $\mathbf{H}(s)$ measurements are available, it is impossible to compute \mathbf{P}_0 , $\mathbf{P}_1 \in \mathbb{R}^{p \times m}$ from (2.12). In this section we explain how we can estimate \mathbf{H}_{poly} and account for it in the Loewner framework. The key assumption is that information about the transfer function is known at high frequency bands. More precisely, we assume that $\mathbf{H}(\iota \omega)$ is known for large positive real numbers ω . Here, denote the imaginary unit with $\iota = \sqrt{-1}$. Since $\lim_{|\omega| \to \infty} |\mathbf{H}_{\text{spr}}(\iota \omega)| = 0$, the contribution of the strictly proper part $\mathbf{H}_{\text{spr}}(s)$ to the transfer function $\mathbf{H}(s)$ becomes negligible for high frequency ranges.

4.1 Estimation from One and Two Data Points

Assume that the transfer function $\mathbf{H}(s)$ is known at one point $\iota \eta$ located on the imaginary axis where $\eta \in \mathbb{R}$ and $\eta \gg 1$. Since $\lim_{\eta \to \infty} |\mathbf{H}_{\rm spr}(\iota \eta)| = 0$,

$$\mathbf{H}(\iota \eta) = \mathbf{H}_{\text{spr}}(\iota \eta) + \mathbf{P}_0 + \iota \eta \mathbf{P}_1 \approx \mathbf{P}_0 + \iota \eta \mathbf{P}_1.$$

This gives the estimates

$$\widehat{\mathbf{P}}_0 = \operatorname{Re}(\mathbf{H}(\iota \, \eta)), \qquad \widehat{\mathbf{P}}_1 = \eta^{-1} \operatorname{Im}(\mathbf{H}(\iota \, \eta)).$$
 (4.1)

Next, assume that the transfer function $\mathbf{H}(s)$ is known for two points $\iota \eta$ and $\iota \theta$ on the imaginary axis with $\eta, \theta \in \mathbb{R}$ and $\theta > \eta \gg 1$. We have

$$\mathbf{H}(\iota \,\theta) - \mathbf{H}(\iota \,\eta) = \left(\mathbf{H}_{\mathrm{spr}}(\iota \,\theta) + \mathbf{P}_0 + \iota \,\theta \mathbf{P}_1\right) - \left(\mathbf{H}_{\mathrm{spr}}(\iota \,\eta) + \mathbf{P}_0 + \iota \,\eta \mathbf{P}_1\right)$$
$$= \mathbf{H}_{\mathrm{spr}}(\iota \,\theta) - \mathbf{H}_{\mathrm{spr}}(\iota \,\eta) + (\iota \,\theta - \iota \,\eta)\mathbf{P}_1 \approx (\iota \,\theta - \iota \,\eta)\mathbf{P}_1. \tag{4.2}$$

Hence, we can estimate P_1 in terms of a divided difference value that appears in the Loewner matrix with $\lambda = \iota \eta$ and $\mu = \iota \theta$ (that is approximating the derivative when $\theta \to \eta$), as follows

$$\widehat{\mathbf{P}}_{1} = \operatorname{Re}\left(\frac{\mathbf{H}(\iota \, \theta) - \mathbf{H}(\iota \, \eta)}{\iota \, \theta - \iota \, \eta}\right). \tag{4.3a}$$

We also have

$$i \theta \mathbf{H}(i \theta) - i \eta \mathbf{H}(i \eta)$$

$$= \left(i \theta \mathbf{H}_{spr}(i \theta) + i \theta \mathbf{P}_0 - \theta^2 \mathbf{P}_1\right) - \left(i \eta \mathbf{H}_{spr}(i \eta) + i \eta \mathbf{P}_0 - \eta^2 \mathbf{P}_1\right)$$

$$= i \theta \mathbf{H}_{spr}(i \theta) - i \eta \mathbf{H}_{spr}(i \eta) + (i \theta - i \eta) \mathbf{P}_0 + (\eta^2 - \theta^2) \mathbf{P}_1,$$

which implies

$$\frac{\iota \, \theta \mathbf{H}(\iota \, \theta) - \iota \, \eta \mathbf{H}(\iota \, \eta)}{\iota \, \theta - \iota \, \eta} = \frac{\iota \, \theta \mathbf{H}_{\text{spr}}(\iota \, \theta) - \iota \, \eta \mathbf{H}_{\text{spr}}(\iota \, \eta)}{\iota \, \theta - \iota \, \eta} + \mathbf{P}_0 + \iota (\eta + \theta) \mathbf{P}_1$$
$$\approx \mathbf{P}_0 + \iota (\eta + \theta) \mathbf{P}_1.$$

The previous approximation gives the following estimate for P_0 ,

$$\widehat{\mathbf{P}}_0 = \operatorname{Re}\left(\frac{\iota \,\theta \mathbf{H}(\iota \,\theta) - \iota \,\eta \mathbf{H}(\iota \,\eta)}{\iota \,\theta - \iota \,\eta}\right). \tag{4.3b}$$

Example 4.1 Consider the order n = 3 DAE system

$$\underbrace{\begin{bmatrix} 1 & 0 \\ 0 & 1 \end{bmatrix}}_{\mathbf{E}_{11}} \frac{d}{dt} \mathbf{v}(t) = \underbrace{\begin{bmatrix} 1 & 0 \\ 0 & 2 \end{bmatrix}}_{\mathbf{A}_{11}} \mathbf{v}(t) + \underbrace{\begin{bmatrix} 1 \\ 0 \end{bmatrix}}_{\mathbf{A}_{12}} \mathbf{p}(t) + \underbrace{\begin{bmatrix} 1 & -1 \\ 1 & 1 \end{bmatrix}}_{\mathbf{B}_{1,0}} \mathbf{g}(t),$$

$$\mathbf{0} = \underbrace{\begin{bmatrix} 1 & 0 \end{bmatrix}}_{\mathbf{A}_{12}^T} \mathbf{v}(t) + \underbrace{\begin{bmatrix} 1 & 2 \end{bmatrix}}_{\mathbf{B}_{2,0}} \mathbf{g}(t),$$

$$\mathbf{y}(t) = \underbrace{\begin{bmatrix} 2 & 1 \\ 0 & 1 \end{bmatrix}}_{\mathbf{C}_1} \mathbf{v}(t) + \underbrace{\begin{bmatrix} 3 \\ 1 \end{bmatrix}}_{\mathbf{C}_2} \mathbf{p}(t),$$

which is of the form (1.1), with $\mathbf{B}_{1,1} = \mathbf{D}_0 = \mathbf{D}_1 = \mathbf{0}_{2\times 2}$. For this small example we can compute the transfer function explicitly, e.g., using the symbolic toolbox in Matlab applied to (2.1), to get

$$\mathbf{H}_{\mathrm{spr}}(s) = \frac{1}{s-2} \begin{bmatrix} 1 & 1 \\ 1 & 1 \end{bmatrix}, \qquad \mathbf{H}_{\mathrm{poly}}(s) = \underbrace{\begin{bmatrix} -2 & 5 \\ 0 & 3 \end{bmatrix}}_{=\mathbf{P}_0} + s \underbrace{\begin{bmatrix} -3 & -6 \\ -1 & -2 \end{bmatrix}}_{=\mathbf{P}_1}. \tag{4.5}$$

First, we estimate P_0 and P_1 in (4.5) from one measurement pair $(\iota \eta, \mathbf{H}(\iota \eta))$ using (4.1). In this simple example, these errors can be computed analytically from (4.5) and happen to be nearly identical,

$$\mathbf{P}_0 - \widehat{\mathbf{P}}_0 = \mathbf{P}_0 - \operatorname{Re}\left(\mathbf{H}(\iota \, \eta)\right) = \frac{2}{\eta^2 + 4} \begin{bmatrix} 1 & 1 \\ 1 & 1 \end{bmatrix} = O(\eta^{-2}),$$

$$\mathbf{P}_1 - \widehat{\mathbf{P}}_1 = \mathbf{P}_1 - \eta^{-1} \operatorname{Im}\left(\mathbf{H}(\iota \, \eta)\right) = \frac{1}{\eta^2 + 4} \begin{bmatrix} 1 & 1 \\ 1 & 1 \end{bmatrix} = O(\eta^{-2}).$$

The errors for different η are depicted by the black curves with crosses in Fig. 1.

Next, we estimate the values of \mathbf{P}_0 and \mathbf{P}_1 in (4.5) from two measurement pairs $(\iota \eta, \mathbf{H}(\iota \eta))$ and $(\iota \theta, \mathbf{H}(\iota \theta))$ using the estimates (4.3). Specifically, we use the second frequency $\theta = 10 \eta$ or $\theta = 100 \eta$. The errors $\|\mathbf{P}_0 - \widehat{\mathbf{P}}_0\|_2$ are shown in the left plot in Fig. 1, while the errors $\|\mathbf{P}_1 - \widehat{\mathbf{P}}_1\|_2$ are shown in the right plot. The red curves with circles correspond to the estimates (4.3) with $\theta = 10 \eta$ and green curves with diamonds correspond to the estimates (4.3) with $\theta = 100 \eta$. Again, the errors behave like $O(\eta^{-2})$. Adding a second frequency $\theta = 10^k \eta$, k = 1, 2, reduces the error approximately by 10^{-k} .

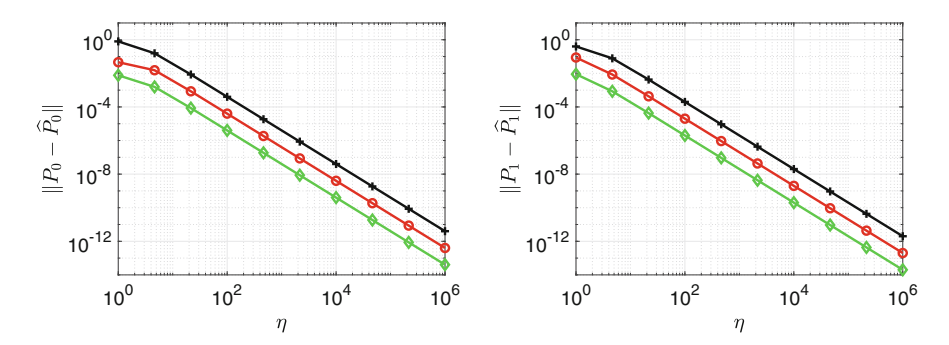


Fig. 1 Errors $\|\mathbf{P}_0 - \widehat{\mathbf{P}}_0\|_2$ (left plot) and $\|\mathbf{P}_1 - \widehat{\mathbf{P}}_1\|_2$ (right plot) for $\widehat{\mathbf{P}}_0$, $\widehat{\mathbf{P}}_1$ estimated from (4.1) and (4.3). The black curves with crosses show the error for the estimates obtained from (4.1) for $\eta \in [10^0, 10^6]$. The red curves with circles and green curves with diamonds show the error for the estimates obtained from (4.3) for $\eta \in [10^0, 10^6]$ and $\theta = 10 \eta$ (red curves with circles) or $\theta = 100 \eta$ (green curves with diamonds). The errors behave like $O(\eta^{-2})$ and adding a second frequency $\theta = 10^k \eta$, k = 1, 2, reduces the error by approximately by 10^{-k}

4.2 Estimation from 2L Data Points—The General Case

Now assume that we have 2L measurements available with sampling points located in high frequency bands, i.e., on the imaginary axis with high absolute value. We will extend the formulas in (4.3) to the general case $L \ge 1$ using the definitions of the Loewner matrices in (3.5) and (3.6).

The set-up is as in Sect. 3. The left interpolation points $\{\iota \ \theta_i\}_{i=1}^L$ and right interpolation points $\{\iota \ \eta_j\}_{j=1}^L$ are chosen on the imaginary axis $\iota \ \mathbb{R}$ with $\min\{\theta_i\}, \min\{\eta_j\} \gg 1$. The goal is to estimate the coefficient matrices $\mathbf{P}_0, \mathbf{P}_1$ taking into account all 2L measurements, and not only two of them as in (4.3).

We begin by extending (4.3a) for the estimation of \mathbf{P}_1 . We write the (i, j) entry of the Loewner matrix \mathbb{L} (3.5) with $\lambda = \iota \eta$ and $\mu = \iota \theta$. Instead of the generic notation \mathbb{L} for the Loewner matrix, we now use the notation \mathbb{L}^{hi} to indicate that this Loewner matrix is computed with data located in high frequency bands, and to later differentiate it from the Loewner matrix \mathbb{L}^{lo} obtained from the remaining data in low frequency band.

Using the equalities (3.3) and (4.2), it follows that the (i, j) entry of the Loewner matrix \mathbb{L}^{hi} (3.5) with $\lambda = \iota \eta$ and $\mu = \iota \theta$ has the expression

$$\mathbb{L}_{(i,j)}^{\text{hi}} = \frac{\mathbf{v}_{i}^{*}\mathbf{r}_{j} - \boldsymbol{\ell}_{i}^{*}\mathbf{w}_{j}}{\iota \, \theta_{i} - \iota \, \eta_{j}} = \frac{\boldsymbol{\ell}_{i}^{*}\mathbf{H}(\iota \, \theta_{i})\mathbf{r}_{j} - \boldsymbol{\ell}_{i}^{*}\mathbf{H}(\iota \, \eta_{j})\mathbf{r}_{j}}{\iota \, \theta_{i} - \iota \, \eta_{j}} = \boldsymbol{\ell}_{i}^{*} \left(\frac{\mathbf{H}(\iota \, \theta_{i}) - \mathbf{H}(\iota \, \eta_{j})}{\iota \, \theta_{i} - \iota \, \eta_{j}}\right) \mathbf{r}_{j}$$

$$= \boldsymbol{\ell}_{i}^{*} \left(\frac{\mathbf{H}_{\text{spr}}(\iota \, \theta_{i}) - \mathbf{H}_{\text{spr}}(\iota \, \eta_{j}) + (\iota \, \theta_{i} - \iota \, \eta_{j})\mathbf{P}_{1}}{\iota \, \theta_{i} - \iota \, \eta_{j}}\right) \mathbf{r}_{j}$$

$$= \underline{\boldsymbol{\ell}_{i}^{*}} \left(\frac{\mathbf{H}_{\text{spr}}(\iota \, \theta_{i}) - \mathbf{H}_{\text{spr}}(\iota \, \eta_{j})}{\iota \, \theta_{i} - \iota \, \eta_{j}}\right) \mathbf{r}_{j}} + \boldsymbol{\ell}_{i}^{*}\mathbf{P}_{1}\mathbf{r}_{j} = \mathbb{L}_{(i,j)}^{\text{hi,spr}} + \boldsymbol{\ell}_{i}^{*}\mathbf{P}_{1}\mathbf{r}_{j}. \tag{4.6}$$

As in (3.4), the directional vectors ℓ_i and \mathbf{r}_i are collected into matrices

$$(\mathbf{L}^{\text{hi}})^* = \begin{bmatrix} \boldsymbol{\ell}_1 \ \boldsymbol{\ell}_2 \cdots \boldsymbol{\ell}_L \end{bmatrix} \in \mathbb{C}^{p \times L}, \qquad \mathbf{R}^{\text{hi}} = \begin{bmatrix} \mathbf{r}_1 \ \mathbf{r}_2 \cdots \mathbf{r}_L \end{bmatrix} \in \mathbb{C}^{m \times L}.$$
 (4.7)

Combining (4.6) and (4.7) gives the approximation formula

$$\mathbb{L}^{\text{hi}} = \mathbb{L}^{\text{hi},\text{spr}} + \mathbf{L}^{\text{hi}} \mathbf{P}_1 \mathbf{R}^{\text{hi}} \approx \mathbf{L}^{\text{hi}} \mathbf{P}_1 \mathbf{R}^{\text{hi}}, \tag{4.8}$$

again obtained by neglecting the contribution of the strictly proper part of the transfer function at high frequencies.

Provided that $L \ge \max\{p, m\}$ (recall that here m is the number of inputs and p is the number of outputs), one can write the estimated linear polynomial coefficient matrix as follows

$$\widehat{\mathbf{P}}_{1} = \text{Re}\left(\left(\mathbf{L}^{\text{hi}}\right)^{\dagger} \mathbb{L}^{\text{hi}} \left(\mathbf{R}^{\text{hi}}\right)^{\dagger}\right), \tag{4.9a}$$

where $\mathbf{X}^{\dagger} \in \mathbb{C}^{v \times u}$ is the Moore-Penrose pseudo-inverse of $\mathbf{X} \in \mathbb{C}^{u \times v}$.

Similarly to the procedure used for estimating \mathbf{P}_1 , one can extend the formula in (4.3b) for estimating \mathbf{P}_0 from the shifted Loewner matrix $\mathbb{L}_s^{\mathrm{hi}}$ computed from L sampling points located in high frequency bands as follows

$$\widehat{\mathbf{P}}_{0} = \operatorname{Re}\left(\left(\mathbf{L}^{\operatorname{hi}}\right)^{\dagger} \mathbb{L}_{s}^{\operatorname{hi}}\left(\mathbf{R}^{\operatorname{hi}}\right)^{\dagger}\right). \tag{4.9b}$$

4.3 The Proposed Procedure

Assume that we have samples of the transfer function evaluated at high frequencies (to capture the polynomial part) as well as at low frequencies (to capture the strictly proper part). Algorithm 1 below adapts the Loewner framework for DAE systems by preserving the polynomial structure of the underlying transfer function. The ROM constructed with Algorithm 1 has the form

$$\widehat{\mathbf{E}}\frac{d}{dt}\widehat{\mathbf{x}}(t) = \widehat{\mathbf{A}}\widehat{\mathbf{x}}(t) + \widehat{\mathbf{B}}_0 \mathbf{g}(t), \qquad t \in (0, T), \tag{4.10a}$$

$$\widehat{\mathbf{E}}\widehat{\mathbf{x}}(0) = \mathbf{0},\tag{4.10b}$$

$$\widehat{\mathbf{y}}(t) = \widehat{\mathbf{C}}\widehat{\mathbf{x}}(t) + \widehat{\mathbf{P}}_0 \,\mathbf{g}(t) + \widehat{\mathbf{P}}_1 \frac{d}{dt} \mathbf{g}(t), \qquad t \in (0, T). \tag{4.10c}$$

The derivative $\frac{d}{dt}\mathbf{g}(t)$ is not an explicit input into the dynamics (4.10a), i.e., $\widehat{\mathbf{R}}_1 = \mathbf{0}$, but its influence on the output is modeled by the feed-through term $\widehat{\mathbf{P}}_1 \frac{d}{dt}\mathbf{g}(t)$ in the output equation (4.10c). While some structural details of the ROM (4.10) are

different from the original FOM (1.3), the transfer function

$$\widehat{\mathbf{H}}(s) = \widehat{\mathbf{H}}_{\text{spr}}(s) + \widehat{\mathbf{H}}_{\text{poly}}(s)$$
 (4.11a)

of the ROM (4.10), now has a strictly proper part and a polynomial part,

$$\widehat{\mathbf{H}}_{\mathrm{spr}}(s) = \widehat{\mathbf{C}}(s\,\widehat{\mathbf{E}} - \widehat{\mathbf{A}})^{-1}\widehat{\mathbf{B}}_{0}, \quad \widehat{\mathbf{H}}_{\mathrm{poly}}(s) = \widehat{\mathbf{P}}_{0} + s\,\widehat{\mathbf{P}}_{1}.$$
 (4.11b)

Numerical experiments indicate that each of these match the ones of the FOM (2.12) well, provided enough transfer measurements are available.

Instead of the generic λ_j , $\mu_j \in \mathbb{C}$ used in Sect. 3 we now specify $\lambda_j = \iota \eta_j$ and $\mu_j = \iota \theta_j$ in Algorithm 1 with η_j , $\theta_j \in \mathbb{R}$.

Algorithm 1 Modified Loewner method with identification of polynomial terms in transfer function

Input: A data set composed of 2(N + L) sample points, 2(N + L) tangential directions, and 2(N + L) measured values of the transfer function as introduced in (3.1).

Output: Loewner ROM specified by $\widehat{\mathbf{E}}$, $\widehat{\mathbf{A}}$, $\widehat{\mathbf{B}}$, $\widehat{\mathbf{C}}$, $\widehat{\mathbf{P}}_0$, $\widehat{\mathbf{P}}_1$.

- 1: Split the data into 2N data corresponding to the low frequency range and into 2L data corresponding to the high frequency range.
- 2: Use the 2L data corresponding to the high frequency range to estimate $\widehat{\mathbf{P}}_0$, $\widehat{\mathbf{P}}_1$ using (4.9).
- 3: Adjust the 2N transfer function measurements corresponding to the low frequency range, by subtracting the estimated polynomial part $\widehat{\mathbf{H}}_{\text{poly}}(\omega) = \widehat{\mathbf{P}}_0 + \iota \, \omega \, \widehat{\mathbf{P}}_1$ for $\omega \in \{\theta_i \mid 1 \leq i \leq N\} \cup \{\eta_i \mid 1 \leq j \leq N\}$ from the original measurement values, i.e., compute

left:
$$(\iota \theta_j, \boldsymbol{\ell}_j, \mathbf{v}_i - \widehat{\mathbf{H}}_{poly}(\iota \theta_j)^* \boldsymbol{\ell}_j), \quad j = 1, \dots, N,$$

right: $(\iota \eta_j, \mathbf{r}_j, \mathbf{w}_j - \widehat{\mathbf{H}}_{poly}(\iota \eta_j) \mathbf{r}_j), \quad j = 1, \dots, N.$

$$(4.39)$$

- 4: Use the 2N data (4.39) to construct data matrices $\mathbf{V}^{\text{lo}} \in \mathbb{C}^{N \times m}$, $\mathbf{W}^{\text{lo}} \in \mathbb{C}^{p \times N}$ as in (3.4), and Loewner matrices \mathbb{L}^{lo} , $\mathbb{L}_s^{\text{lo}} \in \mathbb{C}^{N \times N}$ as in (3.5) and (3.6).
- 5: Compute the SVD of the augmented Loewner matrices obtained with \mathbb{L}^{lo} , \mathbb{L}_s^{lo} and project as in (3.9) to construct $\widehat{\mathbf{E}} = -\widehat{\mathbb{L}}^{lo} = -\mathbf{Y}^*\mathbb{L}^{lo}\mathbf{X}$, $\widehat{\mathbf{A}} = -\widehat{\mathbb{L}}^{lo}_s = -\mathbf{Y}^*\mathbb{L}^{lo}_s\mathbf{X}$, $\widehat{\mathbf{B}}_0 = \widehat{\mathbf{V}}^{lo} = \mathbf{Y}^*\mathbf{V}^{lo}$, $\widehat{\mathbf{C}} = \widehat{\mathbf{W}}^{lo} = \mathbf{W}^{lo}\mathbf{X}$.

5 Numerical Example—Oseen Equations

In this section we apply the Loewner framework to the Oseen equations. The example specifications are from [8].

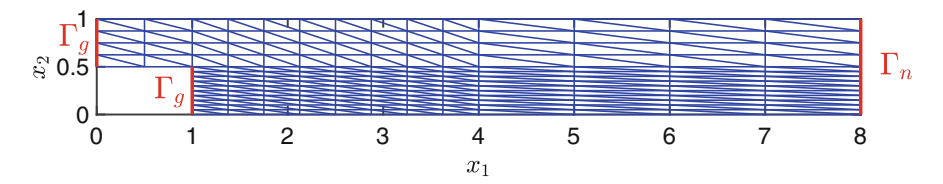


Fig. 2 The channel geometry and coarse grid

5.1 Problem Specification

For completeness we first review the main problem specifications. Let $\Omega \subset \mathbb{R}^2$ be the backward facing step geometry shown in Fig. 2. The boundary is decomposed into segments Γ_n , Γ_d , Γ_g , where $\Gamma_n = \{8\} \times (0, 1)$ is the outflow boundary, inputs are applied on $\Gamma_g = \{0\} \times (1/2, 1) \cup \{1\} \times (0, 1/2)$, and the velocities are set to zero on $\Gamma_d = \partial \Omega \setminus (\Gamma_g \cup \Gamma_n)$.

We consider the Oseen equations

$$\begin{split} \frac{\partial}{\partial t} v(x,t) + (a(x) \cdot \nabla) v(x,t) - v \Delta v(x,t) + \nabla p(x,t) &= 0 & \text{in } \Omega \times (0,T), \\ \nabla \cdot v(x,t) &= 0 & \text{in } \Omega \times (0,T), \\ (-p(x,t)I + v \nabla v(x,t)) n(x) &= 0 & \text{on } \Gamma_n \times (0,T), \\ v(x,t) &= 0 & \text{on } \Gamma_d \times (0,T), \\ v(x,t) &= g_{\varGamma}(x,t) & \text{on } \Gamma_g \times (0,T), \\ v(x,0) &= 0 & \text{in } \Omega, \end{split}$$

where v=1/50 is the dynamic viscosity and where n(x) is the unit outward normal to Ω at x. Here v, p are the velocity and pressure of the fluid respectively, and g_{Γ} denotes the boundary input. The advection field a is computed as in [8, Sec. 7.2] by solving the steady-state Stokes equation with velocity $8(x_2-1/2)(1-x_2)$ on the inflow boundary segment $\Gamma_{in}=\{0\}\times(1/2,1)$ and and zero velocity boundary conditions on $\partial\Omega\setminus(\Gamma_n\cup\Gamma_{in})$.

Our boundary inputs are given as in [8] by

$$g_{\Gamma}(x,t) = \sum_{k=1}^{n_g} \mathbf{g}_k(t) \boldsymbol{\gamma}_k(x)$$
 (5.1)

with $n_g = 6$ boundary control functions $\gamma_j : \mathbb{R}^2 \to \mathbb{R}^2$ given as follows. The first three functions are defined on the inflow boundary segment $\{0\} \times (1/2, 1)$ and are given by

$$\gamma_k(x) = \begin{pmatrix} \sin(2j\pi(x_2 - 1/2)) \\ 0 \end{pmatrix}, \quad k = 1, 2, 3;$$

the remaining three are defined on the backstep boundary segment $\{1\} \times (0, 1/2)$ and are of the form

$$\gamma_{3+k}(x) = \begin{pmatrix} \sin(2j\pi x_2) \\ 0 \end{pmatrix}, \quad k = 1, 2, 3.$$

We use a P1 - P2 Taylor-Hood discretization to arrive at the semi-discrete equations (1.1a-c). (Note that the $\mathbf{B}_{1,1}$ term has accidentally been dropped in [8, Sec. 7.2].) We use a mesh that is obtained from a uniform refinement of the coarse mesh shown in Fig. 2.

We consider the second output from [8, Sec. 7.2], which is the integral of the stress force on the boundary segment $\Gamma_{\text{obs}} = (1, 8) \times \{0\}$,

$$y(t) = \int_{\Gamma_{\text{obs}}} \left(-p(x,t)I + \nu \nabla v(x,t) \right) n(x) ds, \tag{5.2}$$

approximated using the weak form (see [8] for details). This leads to (1.1d) with $C_1 \in \mathbb{R}^{2 \times n_v}$, $C_2 \in \mathbb{R}^{2 \times n_p}$, $D_0 \in \mathbb{R}^{2 \times n_g}$, and $D_1 = 0$. Note that the output matrices represent derivatives of the finite element approximations of velocity v and pressure p and therefore scale with the mesh size h; the finite element approximation of the output y(t) itself does not.

In summary, the semi-discretized DAE model is of dimension $n = n_v + n_p$ with $m = n_g = 6$ inputs and $p = n_y = 2$ outputs.

5.2 Numerical Experiments

We report numerical experiments for a discretization with $n_v = 12,504$ velocity degrees of freedom and $n_p = 1,669$ pressure degrees of freedom. Other discretization sizes gave similar results.

The polynomial coefficient matrices are explicitly computed using the approach in Sect. 2.3 and given by (four digits are shown)

$$\begin{split} \mathbf{P}_0 = \begin{bmatrix} -7.088 & -1.124 \cdot 10^{-4} & -2.363 & -7.731 & -4.172 \cdot 10^{-1} & -2.724 \\ 4.845 \cdot 10^1 & -2.940 \cdot 10^{-4} & 1.615 \cdot 10^1 & 4.927 \cdot 10^1 & 8.727 \cdot 10^{-3} & 1.656 \cdot 10^1 \end{bmatrix}, \\ \mathbf{P}_1 = \begin{bmatrix} -5.484 \cdot 10^{-17} & -2.242 \cdot 10^{-22} & -1.828 \cdot 10^{-17} \\ 7.814 & 1.997 \cdot 10^{-5} & 2.605 \end{bmatrix} \\ -5.576 \cdot 10^{-17} & -4.468 \cdot 10^{-19} & -1.866 \cdot 10^{-17} \\ 7.889 & 3.275 \cdot 10^{-2} & 2.632 \end{bmatrix}. \end{split}$$

Next we compute the Loewner ROM using the classical Loewner approach (3.7) and the modified Loewner approach. For the modified Loewner approach we first modify the transfer function measurements using the true polynomial part $\hat{\mathbf{P}}_0 = \mathbf{P}_0$, $\hat{\mathbf{P}}_1 = \mathbf{P}_1$ computed using the approach in Sect. 2.3. Thus the modified Loewner uses Algorithm 1, with Steps 1 and 2 replaced by the computation of $\hat{\mathbf{P}}_0 = \mathbf{P}_0$, $\hat{\mathbf{P}}_1 = \mathbf{P}_1$ using the approach in Sect. 2.3. We assume that we have 2N = 200 measurements logarithmically spaced in the low frequency range $[10^{-2}, 10^1] \iota$. The left ℓ_j and right \mathbf{r}_j tangential vectors are chosen randomly.

The singular value decay of the Loewner matrices (3.8) computed using measurements in the low frequency range is shown in Fig. 3. The ROM size r is chosen as the largest integer such that $\sigma_r/\sigma_1 > \tau = 10^{-10}$ and is r = 24 for the classical Loewner ROM. In the modified Loewner approach we compute the Loewner matrices from the shifted transfer function measurements (Steps 3+4 in Algorithm 1). The singular value decay of these Loewner matrices is similar the one shown in Fig. 3 and are not plotted. The ROM size r is again chosen as the largest integer such that $\sigma_r/\sigma_1 > \tau = 10^{-10}$ and is r = 23 for the modified Loewner

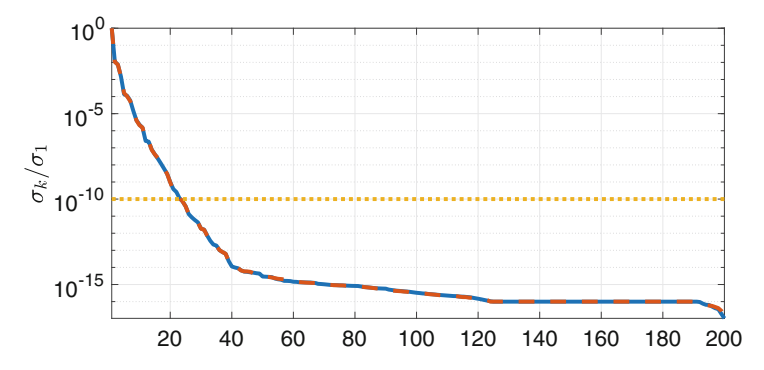


Fig. 3 Singular value decay of the Loewner matrices (3.8) computed using measurements in the low frequency range and tolerance $\tau=10^{-10}$ used to determine the ROM size. The normalized singular values for the two Loewner matrices (3.8) are visually identical

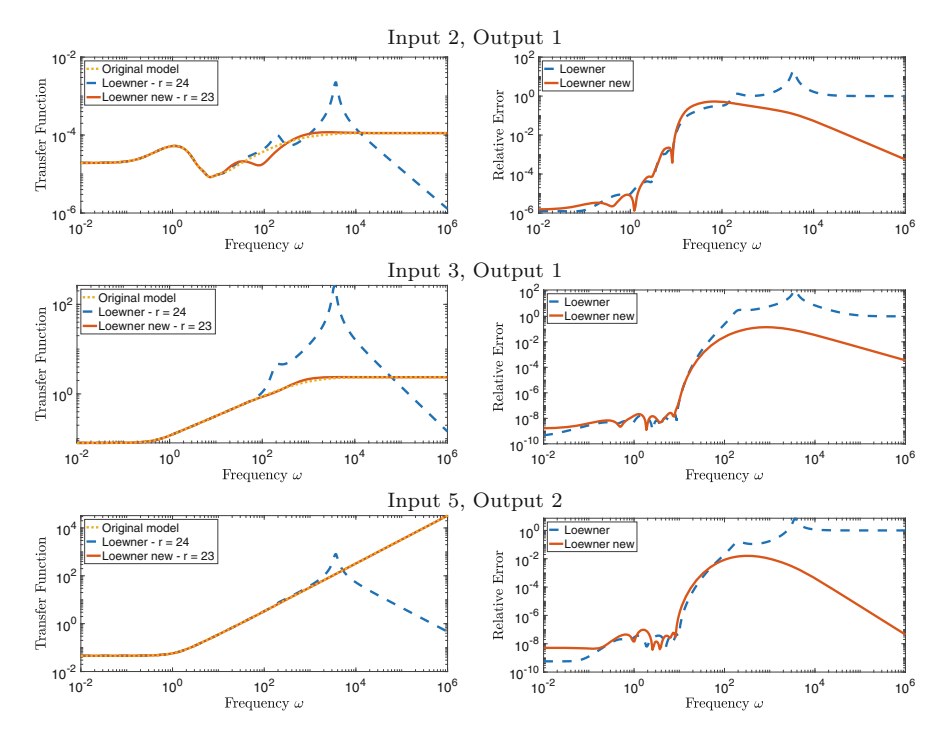


Fig. 4 Left plots: absolute values of frequency responses of the original system (yellow dotted lines) of the reduced system computed with the classical Loewner approach (blue dashed line), and of the reduced system computed with the modified Loewner approach with true $\hat{\mathbf{P}}_0 = \mathbf{P}_0$, $\hat{\mathbf{P}}_1 = \mathbf{P}_1$ (red solid line) for various components of the 2 × 6 transfer function. Loewner ROMs computed using 2N=200 measurements logarithmically spaced in the low frequency range $[10^{-2}, 10^1] \iota$. Right plots: corresponding relative errors

ROM. The left plots in Fig. 4 show the absolute values of frequency responses of the original system (yellow dotted lines) of the reduced system computed with the classical Loewner approach (blue dashed line), and of the reduced system computed with the modified Loewner approach (red solid line) for various components of the 2×6 transfer function at 300 logarithmically spaced frequencies ωt in $[10^{-2}, 10^6]t$. The right plots in Fig. 4 show the corresponding relative errors. We have picked three transfer function components which well represent the overall behavior of the Loewner approach.

The modified Loewner approach generally leads to ROMs with transfer functions that better approximate the true transfer function. The approximation of the transfer function for large frequencies ω is always substantially better when the modified Loewner approach is used. For the transfer function component $\mathbf{H}(i\omega)_{12}$ corresponding to input 2 and output 1 the modified Loewner approach leads to a slightly larger error for frequencies roughly between 10^1 and 10^2 . This is due to the fact that we only use measurements in $[10^{-2}, 10^1]$ ι . If instead we use 2N = 200

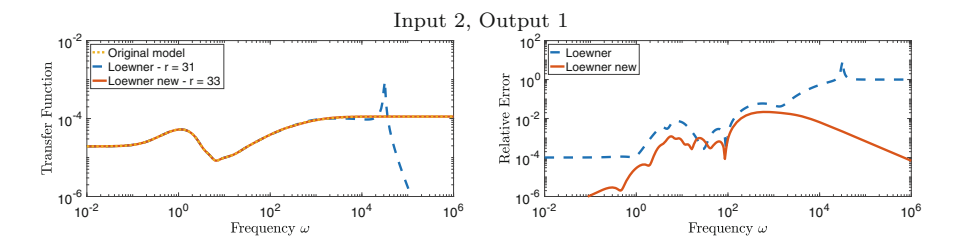


Fig. 5 Left plots: absolute values of frequency responses of the original system (yellow dotted lines) of the reduced system computed with the classical Loewner approach (blue dashed line), and of reduced system computed with the modified Loewner approach with true $\hat{\mathbf{P}}_0 = \mathbf{P}_0$, $\hat{\mathbf{P}}_1 = \mathbf{P}_1$ (red solid line) for the (1, 2) component of the transfer function. Loewner ROMs computed using 2N=200 measurements logarithmically spaced in the low frequency range $[10^{-2}, 10^2]$ ι . Right plots: corresponding relative errors

Table 1 Estimation error for $\widehat{\mathbf{P}}_0$, $\widehat{\mathbf{P}}_1$ computed using (4.9a) and (4.9b) with 2L=20 measurements logarithmically spaced in the high frequency range $[10^f, 10^{f+2}] \iota$ for $f=3,\ldots,7$

Freq. range	$\ \mathbf{P}_0 - \widehat{\mathbf{P}}_0\ _2$	$\ \mathbf{P}_1 - \widehat{\mathbf{P}}_1\ _2$
$[10^3, 10^5]$	$6.0161 \cdot 10^{-2}$	$2.7859 \cdot 10^{-4}$
$[10^4, 10^6]$	$2.5535 \cdot 10^{-4}$	$1.1163 \cdot 10^{-6}$
$[10^5, 10^7]$	$3.0575 \cdot 10^{-6}$	$1.3111 \cdot 10^{-8}$
$[10^6, 10^8]$	$2.8019 \cdot 10^{-8}$	$1.2303 \cdot 10^{-10}$
$[10^7, 10^9]$	$5.8920 \cdot 10^{-10}$	$2.6729 \cdot 10^{-12}$

The observed estimation error for $\hat{\mathbf{P}}_0$ and for $\hat{\mathbf{P}}_1$ behaves like $O(10^{-2}f)$ and in this example the \mathbf{P}_1 estimation error is two orders of magnitude smaller than the \mathbf{P}_0 estimation error

measurements logarithmically spaced in the low frequency range $[10^{-2}, 10^2] \iota$, we get the frequency response in Fig. 5. Approximations for the other transfer function components are also improved when the modified Loewner approach is used, but not plotted because of space limitations. However, note that the classical and modified Loewer ROMs computed using these data are of larger sizes r=31 and r=33. (The ROM size r is again chosen as the largest integer such that $\sigma_r/\sigma_1 > \tau = 10^{-10}$.)

Next we estimate the polynomial part using (4.9a) and (4.9b). Assume that we have 2L = 20 measurements logarithmically spaced in the high frequency range $[10^f, 10^{f+2}] \iota$. The left ℓ_j and right \mathbf{r}_j tangential vectors are chosen randomly. Table 1 shows the estimation error for varying frequency ranges. The observed estimation error for both $\widehat{\mathbf{P}}_0$, $\widehat{\mathbf{P}}_1$ behaves like $O(10^{-2f})$.

In our last experiments we compute the Loewner ROM using the classical Loewner approach (3.7) and the modified Loewner approach, Algorithm 1. Thus, in contrast to the experiments shown in Figs. 4 and 5 we now estimate the polynomial part. Again we assume that we have 2N=200 measurements logarithmically spaced in the low frequency range $[10^{-2}, 10^{1}]$ ι . In addition we assume that we have 2L=20 measurements logarithmically spaced in the high frequency range

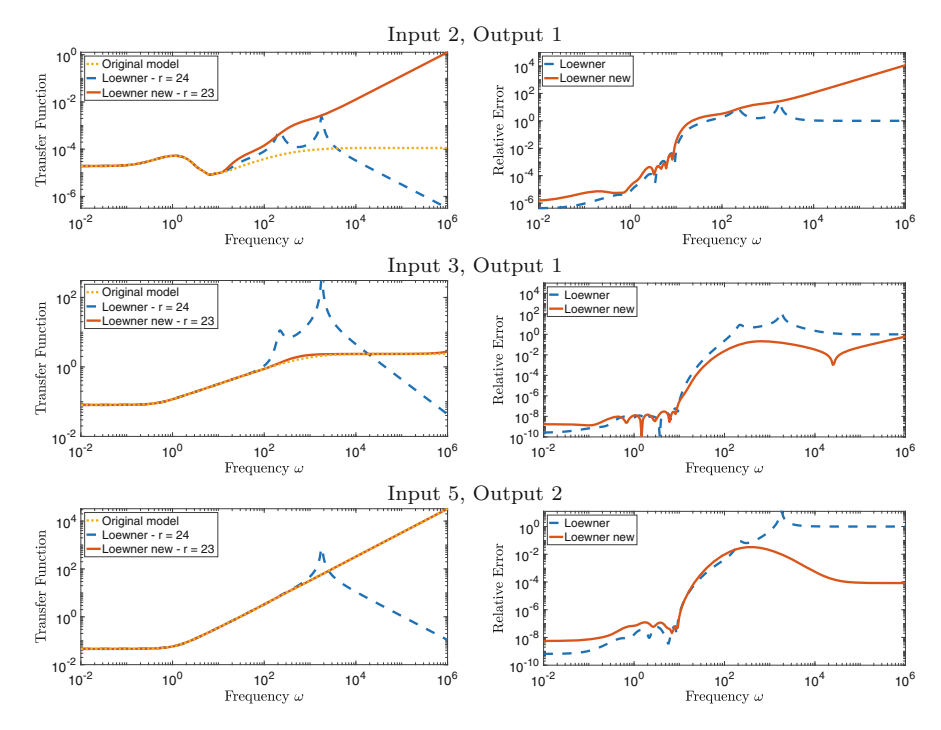


Fig. 6 Left plots: absolute values of frequency responses of the original system (yellow dotted lines) of the reduced system computed with the classical Loewner approach (blue dashed line), and of the reduced system computed with the modified Loewner approach with estimated $\widehat{\mathbf{P}}_0$, $\widehat{\mathbf{P}}_1$ (red solid line) for various components of the 2×6 transfer function. Right plots: corresponding relative errors

[10⁴, 10⁶] ι to compute estimates $\hat{\mathbf{P}}_0$ and $\hat{\mathbf{P}}_1$. In all cases the left ℓ_j and right \mathbf{r}_j tangential vectors are chosen randomly.

The left plots in Fig. 6 show the absolute values of frequency responses of the original system (yellow dotted lines) of the reduced system computed with the classical Loewner approach (blue dashed line), and of reduced system computed with the modified Loewner approach (red solid line) for various components of the 2×6 transfer function at 300 logarithmically spaced frequencies $\omega \iota$ in $[10^{-2}, 10^6]\iota$. The right plots in Fig. 6 show the corresponding relative errors.

In most cases the modified Loewner approach improves the approximation properties of the ROM transfer function. For large frequencies $\omega\gg 1$, the estimation error $\omega\,|(\widehat{\bf P}_1)_{jk}-({\bf P}_1)_{jk}|$ starts to dominate the overall error in transfer function approximation. The beginning of this can be seen in Fig. 6 for Input 3 and Output 1, where the error between FOM transfer function and modified Loewner ROM transfer function begins to grow linearly in ω for $\omega>10^5$. As indicted by Table 1 the errors $\|{\bf P}_0-\widehat{\bf P}_0\|_2$, $\|{\bf P}_1-\widehat{\bf P}_1\|_2$ when 2L measurements at higher frequencies are available to compute $\widehat{\bf P}_0$, $\widehat{\bf P}_1$. Thus while a linear growth in error

between FOM and ROM transfer function is unavoidable when P_1 is present, the impact can be delayed by using measurements at higher frequencies.

The behavior of modified Loewner ROM for the transfer function component corresponding to Input 2 and Output 1 is worse than that of the classical Loewner ROM. Note that this component of the transfer function is substantially smaller than all other components. Moreover, this component of the transfer function has a constant polynomial part, i.e.,

$$\mathbf{H}(\iota \, \omega)_{1,2} = \mathbf{H}_{spr}(\iota \, \omega)_{1,2} + (\mathbf{P}_0)_{1,2}, \quad (\mathbf{P}_0)_{1,2} \approx 10^{-4}, \ (\mathbf{P}_1)_{1,2} = 0,$$

but is estimated by $\widehat{\mathbf{H}}(\iota \, \omega)_{1,2} = \widehat{\mathbf{H}}_{\mathrm{spr}}(\iota \, \omega)_{1,2} + (\widehat{\mathbf{P}}_0)_{1,2} + \iota \, \omega \, (\widehat{\mathbf{P}}_1)_{1,2}$. The errors in the transfer functions for the modified Loewner and the classical Loewner are nearly identical in the range $[10^{-2}, \, 10^1] \, \iota$ where measurements were taken, but both ROM transfer functions have the wrong asymptotics for large frequencies. The difficulty for the modified Loewner approach is that both $(\mathbf{P}_0)_{1,2}$ and $(\mathbf{P}_1)_{1,2}$ are small (in fact $(\mathbf{P}_1)_{1,2} = 0$).

The modified Loewner ROM can be improved somewhat by thresholding. If there is an error estimate τ_0 and τ_1 available such that $|(\mathbf{P}_0)_{j,k} - (\widehat{\mathbf{P}}_0)_{j,k}| \leq \tau_0$ and $|(\mathbf{P}_1)_{j,k} - (\widehat{\mathbf{P}}_1)_{j,k}| \leq \tau_1$, then for small polynomials components with $|(\widehat{\mathbf{P}}_0)_{j,k}| \leq \tau_0$ or $|(\widehat{\mathbf{P}}_1)_{j,k}| \leq \tau_1$, respectively, the estimation error may be as large as the estimated quantity itself. Hence for components with $|(\widehat{\mathbf{P}}_0)_{j,k}| \leq \tau_0$ we set $(\widehat{\mathbf{P}}_0)_{j,k} = 0$, and for components with $|(\widehat{\mathbf{P}}_1)_{j,k}| \leq \tau_1$ we set $(\widehat{\mathbf{P}}_1)_{j,k} = 0$. Unfortunately, currently there is no rigorous error estimate τ_0 and τ_1 available. Motivated by Table 1 we set $\tau_0 = \tau_1 = 10^{-f}$ when the polynomial part is estimated from measurements in the high frequency range $[10^f, 10^{f+2}]$ ι . Specifically, since we have 2L = 20 measurements logarithmically spaced in the high frequency range $[10^4, 10^6]$ ι to compute estimates $\widehat{\mathbf{P}}_0$ and $\widehat{\mathbf{P}}_1$ we set $\tau_0 = \tau_1 = 10^{-4}$. With this thresholding $(\widehat{\mathbf{P}}_1)_{1,k} = 0$, $k = 1, \ldots 6$, and $(\widehat{\mathbf{P}}_1)_{2,2} = 0$. The absolute values of frequency responses for the (1,2) component of the transfer function and corresponding relative errors are shown in Fig. 7. The error in transfer function

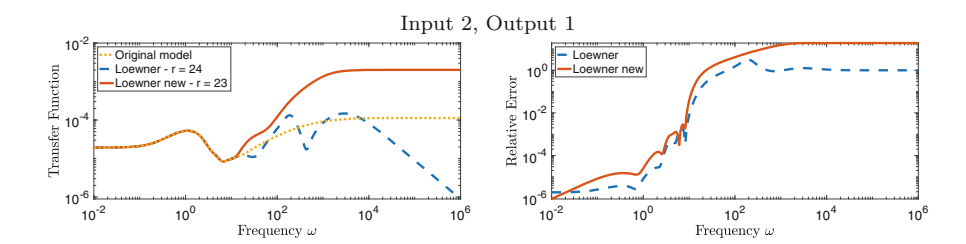


Fig. 7 Left plots: Absolute values of frequency responses of the original system (yellow dotted lines) of the reduced system computed with the classical Loewner approach (blue dashed line), and of the reduced system computed with the modified Loewner approach with estimated $\widehat{\mathbf{P}}_0$, $\widehat{\mathbf{P}}_1$ and thresholding (red solid line) for the (1,2) component of the transfer function. Right plots: corresponding relative errors

for the modified Loewner and the classical Loewner are again nearly identical in the range $[10^{-2}, 10^1]\iota$ where measurements were taken. For large frequencies the observed relative error in the transfer function for the modified Loewner approach is approximately $|(\mathbf{P}_0)_{1,2}-(\widehat{\mathbf{P}}_0)_{1,2}|/|(\mathbf{P}_0)_{1,2}|$, whereas the relative error in the transfer function for the classical Loewner is always asymptotically equal to one. The fundamental issue is that small polynomial components $|(\mathbf{P}_0)_{j,k}|\ll 1$ and especially $|(\mathbf{P}_1)_{j,k}|\ll 1$ need to be estimated with even smaller absolute errors. This is difficult and requires more measurements at higher frequencies.

6 Conclusions

This paper has provided a detailed description of the analytical form of the transfer function for a class of semi-explicit DAE systems, which includes the semi-discretized Oseen equations, and it has introduced a modified version of the data-driven Loewner framework to compute reduced order models (ROMs) for these DAE systems The algorithmic improvement is in the estimation of the polynomial part of the transfer function from measurements and in the incorporation of this estimate into the Loewner ROM construction, which in many cases lead to ROMs with better approximation properties. The modified Loewner approach uses measurements of the transfer function at high frequencies to estimate the polynomial part, and then applies the standard Loewner approach to measurement contributions from the strictly proper part of the transfer function. In particular, the split of the transfer function into a strictly proper and a polynomial part is explicit in the construction of the Loewner ROM to ensure that the resulting ROM transfer function has the same structure. Numerical experiments on the semi-discretized Oseen equations indicate that the modified Loewner approach generates ROMs that better approximate the transfer function if a linear polynomial part is present. In cases, where the polynomial part is linear with a small linear term, the modified Loewner approach can introduce a spurious polynomial part, which then leads to large errors for large frequencies. This can be somewhat avoided by thresholding, but the estimation of small components in the polynomial parts, especially in the linear part remains a difficulty. For the modified Loewner approach precise theoretical error estimates and improvement bounds are not yet available, and are part of future work.

Acknowledgments We thank the referee for carefully reading the paper and providing constructive comments that have lead to a better presentation.

This research was supported in part by NSF grants CCF-1816219 and DMS-1819144.

References

- Antoulas, A.C.: Approximation of large-scale dynamical systems. In: Advances in Design and Control, vol. 6. Society for Industrial and Applied Mathematics (SIAM), Philadelphia (2005). https://doi.org/10.1137/1.9780898718713
- Antoulas, A.C., Lefteriu, S., Ionita, A.C.: Chapter 8: a tutorial introduction to the Loewner framework for model reduction. In: Benner, P., Cohen, A., Ohlberger, M., Willcox, K. (eds.) Model Reduction and Approximation: Theory and Algorithms, pp. 335–376. SIAM, Philadelphia (2017). https://doi.org/10.1137/1.9781611974829.ch8
- Antoulas, A.C., Beattie, C.A., Gugercin, S.: Interpolatory model reduction. In: Computational Science & Engineering, vol. 21. Society for Industrial and Applied Mathematics (SIAM), Philadelphia (2020). https://doi.org/10.1137/1.9781611976083
- Bänsch, E., Benner, P., Saak, J., Weichelt, H.K.: Riccati-based boundary feedback stabilization of incompressible Navier-Stokes flows. SIAM J. Sci. Comput. 37(2), A832–A858 (2015). http://dx.doi.org/10.1137/140980016
- Benner, P., Cohen, A., Ohlberger, M., Willcox, K. (eds.): Model Reduction and Approximation: Theory and Algorithms. Computational Science and Engineering. SIAM, Philadelphia (2017). https://doi.org/10.1137/1.9781611974829
- Elman, H.C., Silvester, D.J., Wathen, A.J.: Finite Elements and Fast Iterative Solvers with Applications in Incompressible Fluid Dynamics. Numerical Mathematics and Scientific Computation, 2nd edn. Oxford University Press, Oxford (2014). http://dx.doi.org/10.1093/acprof: oso/9780199678792.001.0001
- Gosea, I.V., Zhang, Q., Antoulas, A.C.: Preserving the DAE structure in the Loewner model reduction and identification framework. Adv. Comput. Math. 46(1), 3 (2020). https://doi.org/ 10.1007/s10444-020-09752-8
- Heinkenschloss, M., Sorensen, D.C., Sun, K.: Balanced truncation model reduction for a class of descriptor systems with application to the Oseen equations. SIAM J. Sci. Comput. 30(2), 1038–1063 (2008). http://doi.org/10.1137/070681910
- Hesthaven, J.S., Rozza, G., Stamm, B.: Certified Reduced Basis Methods for Parametrized Partial Differential Equations. Springer Briefs in Mathematics. Springer, New York (2015). http://doi.org/10.1007/978-3-319-22470-1
- Layton, W.: Introduction to the Numerical Analysis of Incompressible Viscous Flows. Computational Science & Engineering, vol. 6. Society for Industrial and Applied Mathematics (SIAM), Philadelphia (2008). https://doi.org/10.1137/1.9780898718904
- Mayo, A.J., Antoulas, A.C.: A framework for the solution of the generalized realization problem. Linear Algebra Appl. 425(2–3), 634–662 (2007). https://doi.org/10.1016/j.laa.2007. 03.008
- 12. Quarteroni, A., Manzoni, A., Negri, F.: Reduced basis methods for partial differential equations. An introduction. In: Unitext, vol. 92. Springer, Cham (2016). https://doi.org/10.1007/978-3-319-15431-2